Eur. Phys. J. D **40**, 37–43 (2006)
DOI: 10.1140/epjd/e2006-00130-3

THE EUROPEAN PHYSICAL JOURNAL D

Dynamics of resonant energy transfer in a cold Rydberg gas

S. Westermann, T. Amthor[a], A.L. de Oliveira[b], J. Deiglmayr, M. Reetz-Lamour, and M. Weidemüller[c]

Physikalisches Institut der Universität Freiburg, Hermann-Herder-Str. 3, 79104 Freiburg, Germany

Received 20 December 2005 / Received in final form 3 March 2006
Published online 15 June 2006 –

Abstract. We investigate excitation transfer and migration processes in a cold gas of rubidium Rydberg atoms. Density-dependent measurements of the resonant population exchange for atoms initially excited into the $32P_{3/2}(|m_J| = 3/2)$ state are compared with a Monte Carlo model for coherent energy transfer. The model is based on simulations of small atom subensembles involving up to ten atoms interacting via coherent pair processes. The role of interatomic mechanical forces due to the resonant dipole-dipole interaction is investigated. Good agreement is found between the experimental data and the predictions of the model, from which we infer that atomic motion has negligible influence on the energy transfer up to Rydberg densities of 10^8 cm^{-3}, that the system has to be described in terms of many-body dynamics, and that the energy transfer preserves coherence on microsecond timescales.

PACS. 32.80.Pj Optical cooling of atoms; trapping – 32.80.Rm Multiphoton ionization and excitation to highly excited states – 34.20.Cf Interatomic potentials and forces

1 Introduction

Cold Rydberg gases have opened the possibility to study atomic interaction processes over long timescales and over large distances. Due to the low temperature, the dynamics of the gas is fully determined by the electric dipole interactions between the Rydberg atoms. Two Rydberg pair states can be made energetically degenerate by tuning an external electric field which results in a resonance for the energy and population transfer, known as Förster resonant energy transfer responsible for non-radiative energy redistribution in certain biological systems [1]. As the strength and character of the interaction can be controlled by the electric field [2], one creates an interacting many-body quantum system with controllable couplings which may be useful, e.g., for the implementation of quantum computation [3,4]. By analyzing the line shape of energy transfer resonances for different atomic densities, it was revealed that the dynamics of excitation exchange processes is not governed by simple pair interaction processes, but that migration of excitation requires the system to be described in terms of multi-particle states [5–8]. The Rydberg atoms, prepared out of an ultracold gas, were considered to be stationary in the models presented in those works.

However, the strong long-range interactions can lead to acceleration of the initially stationary atoms on the timescales under consideration. It has been seen that this interaction-induced motion can eventually cause collisions and ionization of the Rydberg atoms [9,10]. In a different approach based on this interaction-induced motion, the resonant energy transfer is described in terms of binary collisions, attributing the population transfer to a crossing of corresponding pair potentials [11,12].

In the present paper we discuss the dynamics of the resonant energy transfer process, and examine in how far motion of the atoms needs to be taken into account in the description. We study the timescales of energy transfer for different Rydberg densities using a Monte Carlo model. In contrast to the approach of references [6,13] the model described here considers all possible pair interactions among the atoms. In Section 2 we explain the model and investigate the influence of different atom configurations, atom densities, and motion of the atoms on the dynamics of the energy transfer process. In Section 3 density-dependent measurements of the population transfer rate are presented and compared to the predictions of the model.

2 Model

2.1 Description of the model

Consider the energy transfer process between a pair of Rydberg atoms

$$p + p \rightarrow s + s' \tag{1}$$

as depicted in Figure 1a. Two atoms initially in the state p undergo an energy transfer process, where one

[a] e-mail: thomas.amthor@physik.uni-freiburg.de
[b] *Permanent address:* Instituto de Física, Universidade de São Paulo, São Carlos, SP 13560-970, Brazil; Departamento de Física, Universidade do Estado de Santa Catarina, Joinville, SC 89223-100, Brazil.
[c] e-mail: matthias.weidemueller@physik.uni-freiburg.de

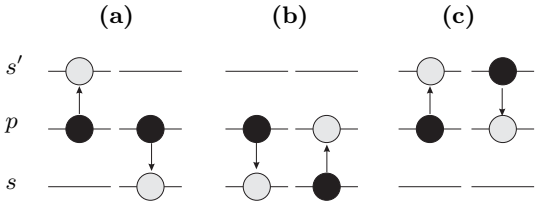

Fig. 1. (a) The resonant energy transfer process 1; (b), (c) the energy exchange processes 2 and 3.

atom is transferred to the energetically lower-lying state s while the other is transferred to the higher-lying state s'. The simplest description of this process is a two-particle model involving the three states $|pp\rangle$, $|ss'\rangle$ and $|s's\rangle$. The states $|ss'\rangle$ and $|s's\rangle$ are energetically separated from $|pp\rangle$ by Δ[1]. The states interact with $V_1(\mathbf{R}) = \langle pp|\hat{V}|ss'\rangle = \langle pp|\hat{V}|s's\rangle = \boldsymbol{\mu}\boldsymbol{\mu}'/|\mathbf{R}|^3 - 3(\boldsymbol{\mu}\mathbf{R})(\boldsymbol{\mu}'\mathbf{R})/|\mathbf{R}|^5$, where $\boldsymbol{\mu} = \langle p|\mathbf{r}|s\rangle$ and $\boldsymbol{\mu}' = \langle p|\mathbf{r}|s'\rangle$ denote the dipole moment matrix elements and $\mathbf{R}$ the distance vector between the two atoms. The dipolar interaction is anisotropic and depends on the angle between the quantization axis (electric field) and $\mathbf{R}$. A resonant energy transfer process occurs for $\Delta = 0$. Experimentally, Δ is set by tuning a static electric field $\mathcal{E}$, which shifts the levels via the Stark effect. The number of s and p atoms can be detected independently by field-selective ionization [14].

In addition to the resonant energy transfer process (1) exchange of excitation between two neighboring atoms is possible via the excitation exchange processes

$$s + p \rightarrow p + s \quad (2)$$

$$s' + p \rightarrow p + s' \quad (3)$$

(see Figs. 1b and 1c) whose interaction strengths are $V_2(\mathbf{R}) = \langle sp|\hat{V}|ps\rangle = \boldsymbol{\mu}^2/|\mathbf{R}|^3 - 3(\boldsymbol{\mu}\mathbf{R})^2/|\mathbf{R}|^5$ and $V_3(\mathbf{R}) = \langle s'p|\hat{V}|ps'\rangle = \boldsymbol{\mu}'^2/|\mathbf{R}|^3 - 3(\boldsymbol{\mu}'\mathbf{R})^2/|\mathbf{R}|^5$. These processes are always resonant and can lead to a migration of an $|ss'\rangle$ pair excitation to neighboring atoms [7,8]. Note that only (1) produces s atoms, while (2) and (3) conserve the number of s atoms. However, as was argued in reference [8], processes (2) and (3) can enhance process (1), particularly at non-vanishing detunings Δ in the following way: for large Δ, only close pairs undergo (1). Subsequent migration processes (2) and (3) which are resonant and therefore active over larger distances put the pair back to $|pp\rangle$, allowing again for (1). Thus, pairs that are accidentally close together are responsible for the line broadening observed and modeled by references [8,13].

The basis for N atoms can be expressed as $|\psi_1\psi_2\psi_3\ldots\psi_N\rangle$, where ψ_i denotes the state of the atom at position i and can be either p, s, or s'. Considering that the number of s and s' atoms must always be the same, this gives a total of three states for two atoms, seven states for three atoms, 19 states for four atoms, 141 states for six atoms, 1107 states for eight atoms, and 8953 states for ten atoms. The corresponding Hamiltonian matrix contains non-zero entries for each pair of states connected via one of the pair interaction processes (1), (2), or (3).

The simulations were performed for the Rydberg states $p = 32\mathrm{P}_{3/2}$, $s = 32\mathrm{S}_{1/2}$ and $s' = 33\mathrm{S}_{1/2}$ of ^{87}Rb, where we calculated the radial dipole matrix elements to be $\mu_{\mathrm{rad}} = 966$ au and $\mu'_{\mathrm{rad}} = 943$ au following reference [15]. As in the experiment described in Section 3, we assumed half of the atoms to be initially in the state $32\mathrm{P}_{3/2}(m_J = +3/2)$ and half in the state $32\mathrm{P}_{3/2}(m_J = -3/2)$. In a spherical basis, the non-zero matrix elements for the transition $32\mathrm{P}_{3/2}(|m_J| = 3/2) \leftrightarrow 32\mathrm{S}_{1/2}$ (including Clebsch-Gordon coefficients) are

$$|\langle 32\mathrm{P}_{\frac{3}{2},\ m_J=+\frac{3}{2}}|\mu_+|32\mathrm{S}_{\frac{1}{2},\ m_J=+\frac{1}{2}}\rangle| = \mu_{\mathrm{rad}}/\sqrt{3} \quad (4)$$

$$|\langle 32\mathrm{P}_{\frac{3}{2},\ m_J=-\frac{3}{2}}|\mu_-|32\mathrm{S}_{\frac{1}{2},\ m_J=-\frac{1}{2}}\rangle| = \mu_{\mathrm{rad}}/\sqrt{3} \quad (5)$$

(accordingly $|\mu'_\pm| = \mu'_{\mathrm{rad}}/\sqrt{3}$ for the transition $32\mathrm{P}_{3/2}(|m_J| = 3/2) \leftrightarrow 33\mathrm{S}_{1/2}$). Note that neither of the processes (1), (2), (3) changes the sign of m_J [2].

To model the time development of the s population, we average over the coherent evolution of subensembles consisting of 4 to 10 atoms using a Monte Carlo method. 1000 atoms at a given average density n are randomly placed in a box. From the center of the box, the smallest sphere containing the desired number of atoms is used to select these atoms as a subensemble. For this specific spatial constellation, initially in the state $|pppp...\rangle$, we numerically solve the time-dependent Schrödinger equation. The anisotropy of the dipole interaction is fully taken into account.

To obtain the number of s atoms produced after some interaction time t one has to add up the probability amplitudes of the respective states at time t multiplied by the number of s atoms contained. This number is then divided by the number of atoms involved in the model, in order to obtain the fraction of atoms in the s state. The inset of Figure 2 shows the time evolution for two different spatial constellations in the six-atom model. This procedure is repeated for a number of realizations of the system and the results are averaged, giving the curves in Figure 2. The number of realizations needed to obtain a smooth graph depends on the number of atoms in the simulation, and for the curves shown here range from 1000 for the ten-atom model to 4000 for the four-atom model.

For comparison, we simulated a two-atom model for which we select atoms out of the random sample in the following way: first, we choose the atom closest to the center of the box. As for each atom the fastest resonant energy transfer occurs with the atom which interacts most strongly, we select the second atom as the one with the strongest interaction (1) to be its partner. For this atom pair we then calculate the probability to be in $|ss'\rangle$ or $|s's\rangle$ and again average over 5000 realizations of the system. Note that a two-atom model cannot involve migration processes (2) and (3).

[1] All expressions in this article are given in atomic units.

[2] Due to the applied electric field, the states with $|m_J| = 1/2$ and $|m_J| = 3/2$ are energetically separated so that the states $32\mathrm{P}_{3/2}(|m_J| = 1/2)$ are not excited and cannot be populated by (1), (2), or (3).

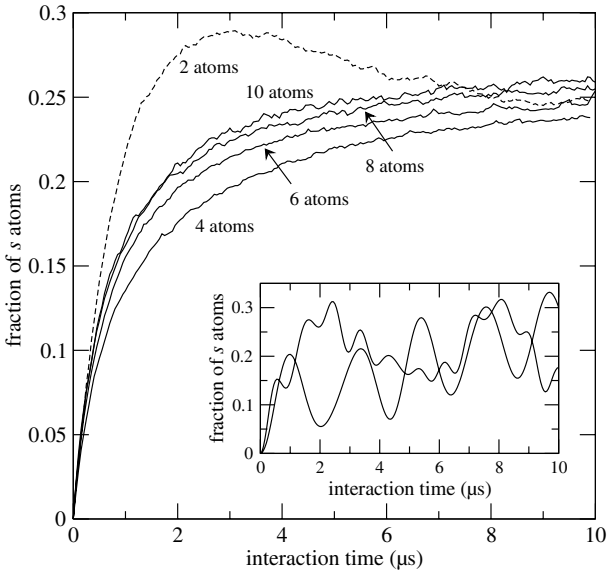

Fig. 2. Comparison of the time development of the s population considering different atom numbers in the model at a density of 10^8 cm^{-3}. The inset shows the coherent evolution of the s population for two specific spatial realizations in the six-atom model. An average over many different realizations yields the curve of the large graph.

The model does not include the spontaneous decay of the involved states (lifetimes around 20–30 μs [14]). To compare the model to experimental data, the graphs presented in Section 3.2 are multiplied with an exponential decay factor.

2.2 Results of the simulation

Figure 2 shows the development of the s-population depending on the number of atoms contained in the subensemble for a density of 10^8 cm^{-3}. Note that the curves were obtained as averages over the time development for different atomic spacings, while the interaction within the interacting set of atoms is described by the model in a fully coherent way. The inset of Figure 2 exemplarily shows the time development of the s population for two specific six-atom constellations. Including more atoms in the model leads to a faster s atom production, which can be explained by the increased probability to have strongly interacting atom pairs in the ensemble considered. All models eventually approach a value of approximately 0.25, corresponding to a 50% probability for each atom to be in the p and 25% to be in the s or s' state, respectively. The differences between the models become less as more atoms are taken into account, suggesting that it is sufficient to consider subensembles of 6–10 atoms to properly model the averaged dynamics of the whole ensemble. For further analysis and to compare with the experiment, we thus chose the six-atom model as a compromise between accuracy and calculational effort. The dashed line in Figure 2 shows the evolution of the s population if only interactions between isolated atom pairs are considered

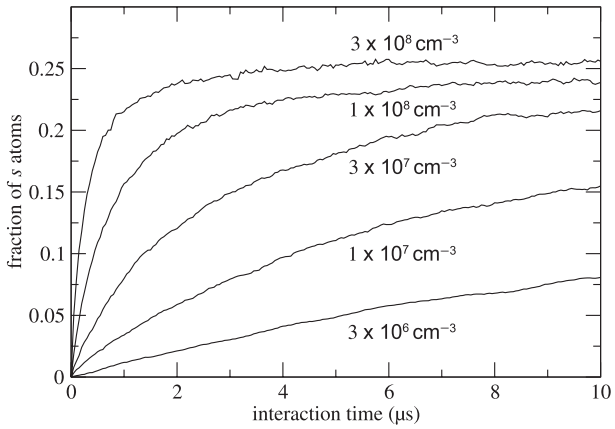

Fig. 3. Dependence of the s population on the interaction time calculated with the six-atom model for different densities.

Table 1. Comparison of the initial transfer rates of the curves depicted in Figure 3.

density n (cm^{-3})	rate γ (μs^{-1})	n/γ (10^8 μs cm^{-3})
3×10^6	0.0112	2.67
1×10^7	0.0423	2.36
3×10^7	0.119	2.52
1×10^8	0.381	2.63
3×10^8	1.201	2.50

(see Sect. 2.1). Here the coherent evolution of the pair states feature Rabi-like oscillations between $|pp\rangle$ and $|ss'\rangle$. The overshoot of the s population visible in this case can be attributed to the fact that the variation of interaction strengths due to the random atom positions is not large enough to completely average out the first oscillation.

In the off-resonance case described in reference [8] the migration processes (2) and (3) enhance the production of s atoms by allowing atom pairs with high interaction strength to undergo the resonant energy transfer (1) several times. On resonance however, the interaction strengths of (1), (2) and (3) are approximately equal. We checked the influence of processes (2) and (3) by performing the same analysis as above for the six-atom model without taking (2) and (3) into account and found no significant difference in the curves. On average, exchanging p and s or p and s' excitation has no effect on the s production when the resonance condition for (1) is fulfilled.

The model shows a clear density dependence of the initial increase of the s population. As the initial population transfer is determined by process (1), the initial transfer rate should be roughly proportional to the average interaction strength $\bar{V}_1$ and thus to the atomic density n due to the $1/R^3$ dependence of V_1. This behavior can indeed be seen in Figure 3 which shows the time development predicted by the six-atom model for a range of experimentally accessible densities. A comparison of the corresponding initial rates is given in Table 1. It is proportional to the density n to a good approximation.

2.3 Motion of the atoms

So far we assumed the atoms to be fixed in space. Initially, this is a very good approximation, as the atoms are prepared at temperatures below 100 μK[3]. However, an attractive C_3/R^3-potential leads to a force between the atoms, which accelerates the atoms towards each other, thus enhancing the coupling V_1 and increasing the transfer rate. Eventually this movement will lead to a collision of the atoms, which is known to evoke a redistribution of the excitation to other Rydberg states or Penning ionization of one of the atoms [9,16].

The time an atom pair initially separated by R_0 needs to collide under the influence of resonant dipole dipole interaction can be calculated as [17]

$$\tau_{\rm coll} = 0.37\sqrt{\frac{m_{\rm Rb}}{C_3}R_0^5}, \tag{6}$$

while the rise time of the s population is on the order of $\tau_{\rm rise} \approx R_0^3/C_3$ (see Sect. 2.2). Thus, one would expect the effect of the atomic motion on the initial rise of the s population to be negligible for $\tau_{coll} \gg \tau_{rise}$ or

$$\frac{\tau_{\rm coll}}{\tau_{\rm rise}} = 0.37\sqrt{\frac{m_{\rm Rb}C_3}{R_0}} \gg 1. \tag{7}$$

Note the weak dependence of (7) on the atomic density n (on average $\tau_{\rm coll}/\tau_{\rm rise} \propto \sqrt[6]{n}$). For $C_3 = 3 \times 10^5$ au, $m_{\rm Rb} = 1.6 \times 10^5$ au and average interatomic separations for densities between 10^6 cm^{-3} and 10^8 cm^{-3} we obtain $\tau_{\rm coll} > 50\tau_{\rm rise}$, so we do not expect the motion of the atoms to have a significant influence on the initial rise of the s population.

We can verify this reasoning by including the motion of the atoms into the model. The motion of the cores in the electronic potential is described purely classically and the discussion is restricted to the most simple system of two atoms with a scalar interaction $V_1(R) = -\mu\mu'/R^3$, solving the time-dependent Schrödinger equation with the time-dependent interaction strength $V_1(t) = V_1(R(t))$ and $R(t)$ obeying Newton's Law

$$\frac{m_{\rm Rb}}{2}\frac{d^2}{dt^2}R(t) = -\frac{d}{dR}V_1(R). \tag{8}$$

This treatment is only valid as long as the electronic wavefunctions of the two atoms are well separated. As the orbital radius of the relevant states is on the order of 1600 a_0 [14], we terminated the calculation once R was below $5500a_0$. Using the same Monte Carlo scheme as above we performed an average over the different interatomic spacings, with atom pairs only contributing to the s population as long as they were separated by more than $5500a_0$. When comparing the results for an atom density of $n = 10^8$ cm^{-3} to the same situation without motion, we find that the initial slope of the s population remains unchanged as expected from (7).

However, as the interaction time increases, atoms are continuously lost due to collisional processes. After 10 μs, about 7% of the atoms are removed from the sample after passing beyond the threshold of minimum distance between the atoms. Although little direct influence of the motion of the atoms on the s population is seen at our simulated densities, a non-negligible fraction of the atoms is predicted to collide at high densities. These collisions can lead to ionization of Rydberg atoms producing free charges [9]. These charges can shift the electric field out of resonance ($\Delta \neq 0$), reducing the rate of s atom production.

Note that only attractive interaction has been considered here. Depending on the orientation of the atoms, repulsive interaction is also possible, which means that the number of dipole interaction-induced collisions estimated here represents an upper limit.

3 Experiment

In order to test the predictions of the model we have performed density-dependent measurements of the dynamics of the energy transfer in a cold cloud of Rydberg atoms.

3.1 Set-up

In a magneto-optical trap (MOT), we prepare cold ^{87}Rb atoms at temperatures on the order of 100 μK. Between 10^7 and 10^8 ^{87}Rb atoms are typically trapped at a peak density of about 10^{10} cm^{-3} with loading times of roughly 5 s. The cold atom cloud is placed between two metal grids (1.5 cm apart) with high optical transmission which are used to apply electric fields. In this way, stray fields can be compensated and the electric field for the energy transfer resonance can be applied. For detection, the Rydberg atoms are field-ionized and the resulting ions are accelerated towards a micro-channel plate detector (MCP).

Excitation to Rydberg states is realized with a a two-photon excitation scheme. The first photon ($5S_{1/2} \rightarrow 5P_{3/2}$, 780 nm) is provided by a high-power diode laser with a linewidth < 1 MHz (Toptica, DLX 110), while the second photon ($5P_{3/2} \rightarrow \mathsf{n}\ell$, 480 nm) is generated by a cw laser system consisting of a frequency-doubled semiconductor laser source with a linewidth <2 MHz (Toptica, TA-SHG 110). The wavelength of this laser can be tuned to address Rydberg levels starting from $\mathsf{n} \simeq 30$ up to the ionization threshold. All lasers can be independently switched by acousto-optical modulators. The frequency of the blue excitation laser is actively stabilized to an ultrastable reference cavity, while the red laser is stabilized via atomic spectroscopy. See references [18,19] for more details.

The two excitation lasers are aligned in a counterpropagating configuration. The red laser ($P_{780\rm nm} = 750$ μW) is collimated to a waist of 1.1 mm, illuminating the whole

[3] 100 μK correspond to a thermal velocity of 0.14 μm/μs, with the average interatomic spacing at a density of 10^8 cm^{-3} being 22 μm.

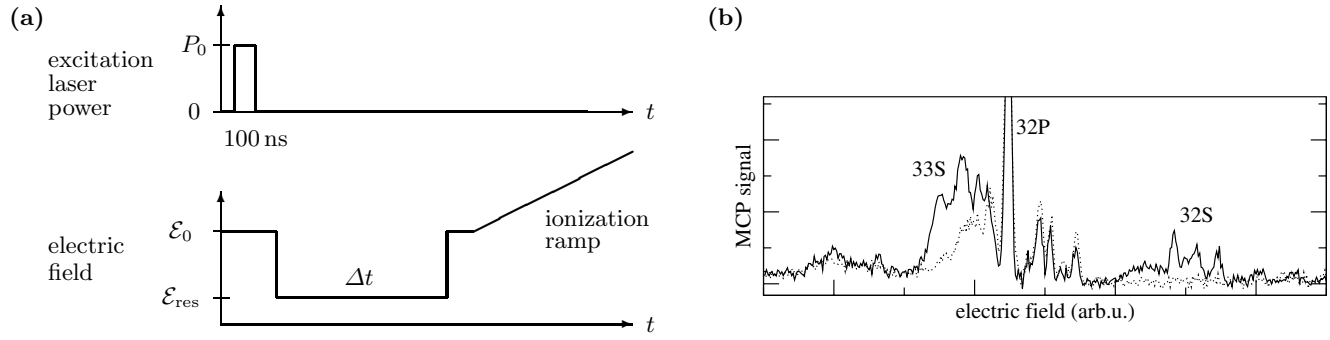

Fig. 4. (a) Timing diagram for the experiment. After a short excitation pulse, the field is switched to the resonance condition at $\mathcal{E}_{\rm res}$ for a time Δt which is varied from 80 ns to 10 μs. Subsequently, the field is ramped up for state-selective field ionization. (b) State-selective field ionization spectra on resonance (solid line, interaction time $\Delta t = 5$ μs) and off resonance (dotted line). Integration windows to determine the population are set on the 32S signal and on the narrow 32P peak which is not displayed in full height here. The 33S signal appears on an underground of the 32P state.

atom cloud, while the blue laser ($P_{480\rm nm} = 30$ mW) is focused to a waist of 37 μm, thus defining the excitation volume. The density of Rydberg atoms can be controlled by varying the population in the $5S_{1/2}(F = 2)$ launch state through optical pumping into the $5S_{1/2}(F = 1)$ state [20].

One experimental cycle (repeated every 70 ms) represents the following timing sequence (see Fig. 4): at time $t = 0$ the excitation laser is switched on for 100 ns. During excitation, the electric field is set to $\mathcal{E}_0 = 15$ V/cm to allow the excitation of the $32P_{3/2}(|m_J| = 3/2)$ state, which is dipole forbidden at zero electric field. This state is spectroscopically resolved due to the narrow bandwidth of the excitation laser. 100 ns after the excitation, the field is switched to $\mathcal{E}_{\rm res} = 11.5$ V/cm for a variable time Δt, which brings the energy transfer process

$$32P_{\frac{3}{2},|m_J|=\frac{3}{2}} + 32P_{\frac{3}{2},|m_J|=\frac{3}{2}} \rightarrow 32S_{\frac{1}{2}} + 33S_{\frac{1}{2}} \qquad (9)$$

into resonance. The field is then switched back to $\mathcal{E}_0$, and 500 ns later it is ramped up to ionize the Rydberg atoms state-selectively. Until the next cycle starts, a high voltage is maintained at the field grids to remove any ions that might be produced during reloading. During excitation and detection, the MOT lasers and the magnetic field are turned off. The field ionization spectra obtained from the MCP detector are averaged over 100–200 shots and the population of the different Rydberg states is determined by integrating the signal over the corresponding time window. In Figure 4b typical spectra for medium density are shown, one without switching to resonance field, the other with an interaction time of $\Delta t = 5$ μs. The redistribution to the 32S and 33S states is clearly visible.

3.2 Comparison with the model

We performed measurements at three different atom densities. The density is varied by switching off the repumping laser for a certain time before excitation, thus optically pumping a certain fraction of the atoms to the dark ground state $5S_{1/2}(F = 1)$ [20]. For the measurements at medium (low) density, the repumping laser is turned off for 5 ms (9 ms) before excitation. This leads to a decrease of ground state atoms available for excitation to 20% (6%) (determined by fluorescence measurements). Assuming a constant excitation rate to the Rydberg state, we can fix the medium and low density relative to the high density n_0 to be 0.2 n_0 and 0.06 n_0.

Figure 5 shows the measured time dependence of the 32P and 32S population at the three different Rydberg atom densities. When the interaction time Δt is zero, only the initially excited 32P atoms are detected. After a few microseconds of interaction, the 32P population has dropped, while some population of the 32S state has accumulated. The remaining atoms have been transferred to the 33S state, which is not shown in the graphs. Clearly the transfer process is faster at higher densities, as is expected from the results in Section 2.2. The decrease of the signals at longer times can be attributed to the lifetime of the Rydberg atoms.

We mapped the number of s atoms obtained from the six-atom model for three densities with fixed ratios $1 : 0.2 : 0.06$ onto the measured number of $32S$ atoms. We found the best agreement of the modeled curves with the experiment for an average density of $n_0 = 2.5 \times 10^8$ cm^{-3}. The spontaneous decay was included by multiplying the predictions of the model by an exponential decay factor $e^{-t/\tau_{\rm eff}}$, where $\tau_{\rm eff} = 24\mu$s denotes the effective lifetime of the Rydberg states[4]. The experimental data have been scaled in height so that the measured s data matches the simulated curve for the s population. The scaling factors are different for the three densities which accounts for the different absolute number of atoms, the saturation behaviour of the MCP, and the fact that some atoms are

[4] Assuming the population transfer to be fast compared to the lifetimes of the involved Rydberg states, the effective decay rate is estimated to be $\tau_{\rm eff}^{-1} = \frac{1}{2}((\tau_{\rm S})^{-1} + (\tau_{\rm P})^{-1}) = (24\ \mu{\rm s})^{-1}$, where $\tau_{\rm S} = 20$ μs and $\tau_{\rm P} = 30$ μs are calculated values for the lifetime of 32S and 32P states at vanishing electric field. These values include spontaneous decay and decay induced by black body radiation [14].

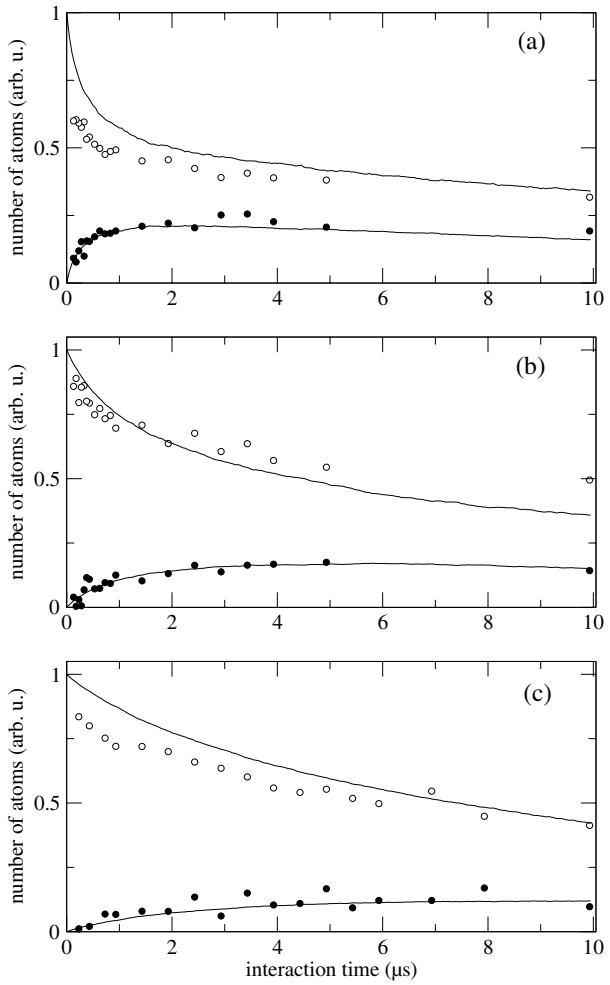

Fig. 5. Measured time dependence of the 32P (○) and 32S (●) population for different Rydberg densities. The solid lines are simulated with the six-atom model for (a) $n = 2.5 \times 10^8$ cm^{-3}, (b) $n = 5 \times 10^7$ cm^{-3} and (c) $n = 1.5 \times 10^7$ cm^{-3}, which correspond to the experimental density ratios of 1 : 0.2 : 0.06.

redistributed to other states [16]. This redistribution causes the effective densities to be less than the total Rydberg densities. We estimate that the ratio between highest and lowest density may actually be up to 40% lower than expected by the experimental settings.

In addition to the s states, the simulated and measured p populations are also shown in Figure 5. The measured data are derived from the central 32P peak in the field ionization spectrum. Since the 32P state also appears at other times in the field ionization spectrum (Fig. 4b), the measured p population is systematically underestimated, as can be seen in Figure 5. The maximum Rydberg density of 2.5×10^8 cm^{-3} determined from the comparison with the simulations is a reasonable value considering the Gaussian density distribution in a MOT with a peak density of 10^{10} cm^{-3} and an excitation probability on the order of 10%.

We also compared the results of the two-atom model to the measured data for a number of different densities. Due to the overshoot visible in Figure 2 it was not possible to find an agreement as good as for the six-atom model. We performed a least squares analysis, yielding substantially better agreement for the six-atom model at the densities chosen in Figure 5 than for any scaling of any modeled density in the two-atom model. This suggests that the behavior of the system must be described in terms of many-body dynamics.

The excitation time has been chosen as short as possible to prevent the production of ions. However, at the highest density presented here, a small number of ions was detected even at short timescales. We find that less than 10% of the Rydberg atoms are ionized in this case, which is in agreement with the number of collisions predicted by the model (see Sect. 2.3). From this we estimate that roughly 10% of the remaining atoms are shifted away from resonance by the electric field of the ions, so that the transfer rate is only slightly affected. In future experiments at higher densities, we will investigate the ion production through collisions and its relevance for the resonant energy transfer in more detail.

4 Conclusion

We have investigated the density dependence of the dynamics of resonant energy transfer processes in a cold Rydberg gas both theoretically in terms of a Monte Carlo model and experimentally by monitoring the number of atoms in the s and p states at different times.

The resonant energy transfer process is modeled by averaging over random realizations of atom ensembles. Resonant energy transfer and excitation exchange processes are allowed between each pair of atoms. We examined the time development of systems with up to ten atoms and found only little difference between models involving six, eight, and ten atoms.

In a second step, motion induced by long-range interaction potentials was included in the model. For the system considered here, this motion was found to have negligible effect on the initial transfer rate. However, the model predicts the motion to lead to ionizing collisions at high densities, which has also been seen in the experiment.

Measurements of the energy transfer evolution were reproduced by the model at three different densities. Satisfying agreement was achieved only by including many-body dynamics. The model describes the time development of the resonant energy transfer in an entirely coherent way. The fact that the model does not predict oscillations is only due to the averaging over different atomic spacing in the disordered atomic cloud as present in a MOT. For a given fixed arrangement of atoms, the system is indeed coherent. Transfer of excitation between the atoms leads to many-body entanglement in this picture. By spatially resolved excitation or by marking specific distances (e.g. via detuned excitation) we hope to produce and detect these many-body states in future experiments. An alternative approach is the combination of an ordered gas of ultracold bosonic ground state atoms in a Mott-insulator state [21] with near-unity excitation of Rydberg atoms through adiabatic passage [22].

The project is supported in part by the Landesstiftung Baden-Württemberg in the framework of the "Quantum Information Processing" program, and a grant from the Ministry of Science, Research and Arts of Baden-Württemberg (Az: 24-7532.23-11-11/1). Exchange with the University of São Paulo is financed by the bilateral PROBRAL program of DAAD and CAPES. We thank T.F. Gallagher for providing us with helpful information and L.G. Marcassa for sending us data for comparison. We are grateful for the remarks of one referee of this paper pointing out that some important interactions were missing in a first version of our model.

References

1. T. Ritz, A. Damjanovi, K. Schulten, Chem. Phys. Chem. **3**, 243 (2002)
2. K. Safinya, J. Delpech, F. Gounand, W. Sandner, T. Gallagher, Phys. Rev. Lett. **47**, 405 (1981)
3. D. Jaksch, J.I. Cirac, P. Zoller, S.L. Rolston, R. Côté, M. Lukin, Phys. Rev. Lett. **85**, 2208 (2000)
4. M.D. Lukin, M. Fleischhauer, R. Côté, L.M. Duan, D. Jaksch, J. Cirac, P. Zoller, Phys. Rev. Lett. **87**, 037901 (2001)
5. V.M. Akulin, F. de Tomasi, I. Mourachko, P. Pillet, Physica D **131**, 125 (1999)
6. W.R. Anderson, M.P. Robinson, J.D.D. Martin, T.F. Gallagher, Phys. Rev. A **65**, 063404 (2002)
7. I. Mourachko, D. Comparat, F. de Tomasi, A. Fioretti, P. Nosbaum, V. Akulin, P. Pillet, Phys. Rev. Lett. **80**, 253 (1998)
8. W.R. Anderson, J.R. Veale, T.F. Gallagher, Phys. Rev. Lett. **80**, 249 (1998)
9. W. Li, P.J. Tanner, T.F. Gallagher, Phys. Rev. Lett. **94**, 173001 (2005)
10. F. Robicheaux, J. Phys. B **38**, S333 (2005)
11. R.A.D.S. Zanon, K.M.F. Magalhães, A.L. de Oliveira, L.G. Marcassa, Phys. Rev. A **65**, 023405 (2002)
12. A.L. de Oliveira, M.W. Mancini, V.S. Bagnato, L.G. Marcassa, Phys. Rev. Lett. **90**, 143002 (2003)
13. I. Mourachko, W. Li, T.F. Gallagher, Phys. Rev. A **70**, 031401 (2004)
14. T.F. Gallagher, *Rydberg Atoms* (Cambridge University Press, Cambridge, 1994)
15. M. Zimmerman, M. Littman, M. Kash, D. Kleppner, Phys. Rev. A **20**, 2251 (1979)
16. A. Walz-Flannigan, J.R. Guest, J.H. Choi, G. Raithel, Phys. Rev. A **69**, 063405 (2004)
17. A. Gallagher, D.E. Pritchard, Phys. Rev. Lett. **63**, 957 (1989)
18. K. Singer, M. Reetz-Lamour, T. Amthor, S. Fölling, M. Tscherneck, M. Weidemüller, J. Phys. B **38**, 321 (2005)
19. M. Reetz-Lamour, T. Amthor, J. Deiglmayr, S. Westermann, K. Singer, A.L. de Oliveira, L.G. Marcassa, M. Weidemüller, Fortschr. Phys. (in press)
20. K. Singer, M. Reetz-Lamour, T. Amthor, L. Marcassa, M. Weidemüller, Phys. Rev. Lett. **93**, 163001 (2004)
21. M. Greiner, O. Mandel, T. Esslinger, T.W. Hänsch, I. Bloch, Nature **415**, 39 (2002)
22. J. Deiglmayr, M. Reetz-Lamour, T. Amthor, S. Westermann, K. Singer, A.L. de Oliveira, M. Weidemüller, Opt. Comm. (in press)